Dalton Transactions

ROYAL SOCIETY OF CHEMISTRY

PAPER

View Article Online
View Journal | View Issue

Cite this: *Dalton Trans.*, 2025, **54**, 5935

Complete ligand substitution and oxidation of the metal center in the photochemical reaction of $CpM(CO)_2I$ (M = Fe, Ru) with chelating β-diketones†

Szymon Jarzyński,[a] Cyprian Doroszko,[a] Daria Jamroz,[a] Kinga Stefanowska-Kątna,[b] Jędrzej Walkowiak,[b] Sławomir Wojtulewski,[c] Janusz Zakrzewski[a] and Bogna Rudolf *[a]

Received 5th February 2025,
Accepted 5th March 2025

DOI: 10.1039/d5dt00294j

rsc.li/dalton

The visible-light irradiation of solutions of $CpFe(CO)_2I$ (Cp = (η^5-C_5H_5)), acetylacetone (or other β-diketones), and diisopropylamine in toluene led to the substitution of all ligands with β-diketonate anions and the oxidation of Fe^{II} to Fe^{III}. The only product was Fe(β-diketonate)$_3$, which exclusively formed even when using an equimolar ratio of $CpFe(CO)_2I$ and diketone. The reaction occurred under both anaerobic and aerobic conditions. The proposed reaction mechanism assigns the key role to the non-innocent behavior of the β-diketonate ligands. Dioxygen or the acetylacetone acts as oxidant. The ruthenium complex $CpRu(CO)_2I$ reacts with acetylacetone in a similar way to the corresponding iron complex, but irradiation with UV light is required to assure an acceptable yield of the product. All obtained complexes were analyzed by NMR, FT-IR, and ESI-MS, and one was subjected to single-crystal and powder X-ray diffraction analysis, which revealed its *mer* stereochemistry.

Introduction

Thermal and photochemical transformations of half-sandwich iron complexes with the formula $CpFe(CO)_2X$ [where Cp = (η^5-C_5H_5) and X = Cl, Br or, most frequently, I] constitute a set of versatile synthetic routes to synthesize various organoiron compounds *via* substitution of the CO and/or X-ligands.[1–10] Some of these compounds display interesting biological activity.[6,7] Visible light photolysis of $CpFe(CO)_2X$ complexes in the presence of neutral 2e ligands (*e.g.*, phosphines) can result in selective CO substitution (Scheme 1).[2,11] This is in contrast to thermal reactions, which often result in competing CO and X substitution. The photolysis of $CpFe(CO)_2I$ (**1a**) in the presence of acidic NH compounds (*e.g.*, pyrroles, indoles, cyclic imides, and sulfonamides) and diisopropylamine (DIPA) leads to substitution of the iodido ligand by the corresponding *N*-anions.[12–17] The photolysis of **1a** in the presence of $Bu_4N^+Y^-$ (Y^- = Br^- or Cl^-) induces halide exchange,[18] while photolysis in the presence of $Bu_4N^+Y^-$ and PPh_3 leads to the tandem substitution of both CO and I^-.

These easy and efficient photochemical substitutions of iodido in **1a** by anions of N–H acids encouraged us to explore similar reactions using β-diketones, which also contain relatively acidic protons and exhibit rich coordination chemistry.[19,20] Surprisingly, we observed that the irradiation of solutions of **1a**, acetylacetone (Hacac, **2a**), and DIPA in toluene led to the substitution of all ligands with β-diketonate anions, giving $Fe(acac)_3$.

Results and discussion

Reaction of the 1a–amine system with acetylacetone (Hacac, 2a)

Irradiation with visible light of an argon-saturated solution of equimolar amounts of **1a** and **2a** and a three-fold excess of DIPA in toluene at 0 °C led to a color change from black to dark red. Monitoring this using thin-layer chromatography (TLC) showed the formation of a dark red compound, which was isolated by column chromatography and identified by elemental analysis and spectroscopy as paramagnetic $Fe^{III}(acac)_3$ (**3a**). This was the only organoiron product (Scheme 2), although there was a significant amount of unreacted **1a**. Furthermore, analysis of volatile components of the reaction mixture using gas chromatography–mass spectrometry (GC-MS) detected cyclopentadiene (*m*/*z* = 66).

[a]*University of Lodz, Faculty of Chemistry, Department of Organic Chemistry, Tamka 12, 91-403 Lodz, Poland. E-mail: bogna.rudolf@chemia.uni.lodz.pl*
[b]*Center for Advanced Technologies, Adam Mickiewicz University, Uniwersytetu Poznańskiego 10, 61-614 Poznań, Poland*
[c]*Department of Structural Chemistry, Faculty of Chemistry, University of Bialystok, Ciołkowskiego 1K, 15-245 Bialystok, Poland*

† Electronic supplementary information (ESI) available: Synthesis of β-diketones, crystallographic data and ^{1}H NMR spectra of compounds **3a–n** and **4**. CCDC 2371792. For ESI and crystallographic data in CIF or other electronic format see DOI: https://doi.org/10.1039/d5dt00294j

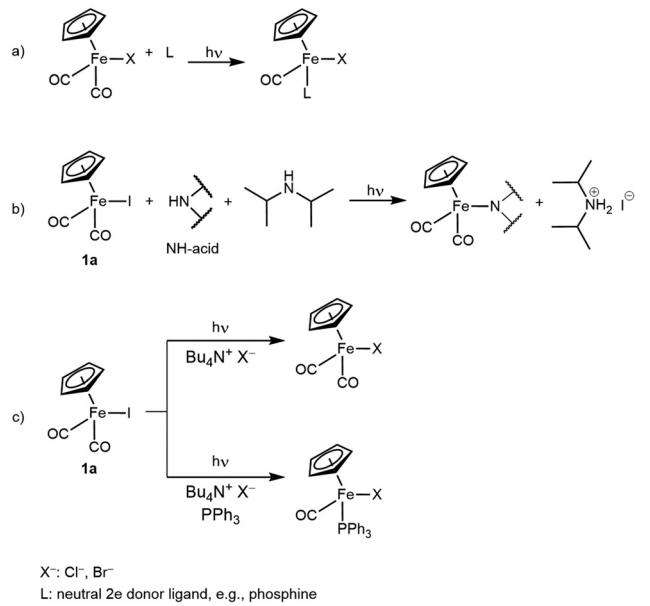

Scheme 1 Photochemical transformations of $CpFe(CO)_2X$: (a) CO ligand exchange,[1,2,6,7,9] (b) photolysis in the presence of acidic NH compounds,[11–16] and (c) photolysis in the presence of $Bu_4N^+Y^-$ with and without PPh_3.[17]

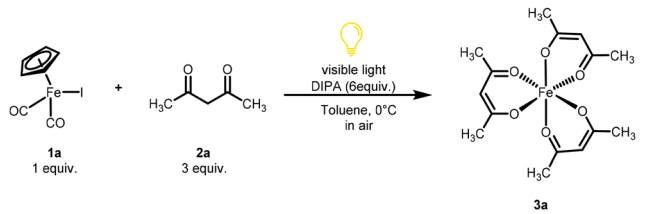

Scheme 2 Photochemical reaction of $CpFe(CO)_2I$ (**1a**) with **2a**.

Repeating the reaction with a ratio of reactants appropriate to the formation of **3a** (*i.e.*, **1a** : **2a** = 1 : 3) and an excess of DIPA achieved practically complete consumption of **1a**, and **3a** was isolated in 73% yield (Table 1, entry 5).

As the reaction involved oxidation of $Fe^{II} \rightarrow Fe^{III}$, we tested whether it would proceed in an oxidizing atmosphere (*i.e.*, air). The presence of air had practically no effect on the course of the reaction or the yield of **3a** (Table 1, entry 1). Therefore, all subsequent experiments were carried out in air. DIPA could be replaced by other amines (*e.g.*, Et_3N, 1,8-diazabicyclo[5.4.0] undec-7-ene (DBU), *N*,*N*-diisopropylethylamine (DIPEA), or pyrrolidine) (Table 1, entries 8–11), but they worked less efficiently. The reaction could also proceed in some other solvents, but less efficiently (Table 1, entries 12–14).

Reactions under aerobic conditions would clearly have dioxygen as the oxidant, with a reduction potential, $E_0^{red} = -0.6$ V ($O_2/O_2^{\bullet-}$ in DMF *vs.* a normal hydrogen electrode).[21] However, the control experiment showed that oxygen is not capable of oxidizing **1a** in either its ground or excited state: the irradiation of this complex in aerated toluene resulted only in its practically quantitative recovery. Hacac displayed even weaker oxidizing properties ($E_0^{red} = -2.2$ V in DMF *vs.* SCE),[22] corresponding to its reduction to $acac^-$ and $\frac{1}{2}$ H_2. This means that the $Fe^{II} \rightarrow Fe^{III}$ oxidation step did not involve **1a**; instead, an intermediate was formed during the reaction. Oxygen is most likely the oxidant in aerobic reactions, while in its absence the weaker oxidant Hacac fulfills this function.

We also used ultraviolet (UV)–visible (vis) and infrared (IR) spectroscopy to observe the solutions of photolyzed aerated **1a** in toluene with Hacac and DIPA in an effort to detect possible intermediates. However, the exclusive formation of **3a** at an equimolar ratio of **1a** and Hacac (Table 1, entry 6) suggests a very rapid transformation of the primary photolysis product with respect to its formation rate.

The spectra in Fig. 1 clearly show that **1a** (λ_{max} = 346 nm) transformed into **3a** (λ_{max} = 354 nm and λ_{max} = 436 nm). The

Table 1 Optimization of the reaction conditions[a]

Entry	Deviation from general conditions	Yield **3a**[b]
1	None	82%
2	No light	N.R.[c]
3	No light, without DIPA	N.R.[c]
4	Sunlight	24%
5	Under argon	73%
6	1 equiv. of **2a** instead of 3 equiv.	62%
7	3 equiv. of DIPA instead of 6 equiv.	69%
8	Et_3N instead of DIPA	43%
9	DBU instead of DIPA	34%
10	DIPEA instead of DIPA	69%
11	Pyrrolidine instead of DIPA	58%
12	THF instead of toluene	47%
13	EtOAc instead of toluene	52%
14	MeOH instead of toluene	28%

[a] General conditions: $CpFe(CO)_2I$ **1a** (1 mmol), acetylacetone **2a** (3 mmol), DIPA (6 mmol), toluene (10 mL), four 100 W tungsten lamps, 1 h, 0 °C. [b] Yield was based on isolated product. [c] N.R. = no reaction.

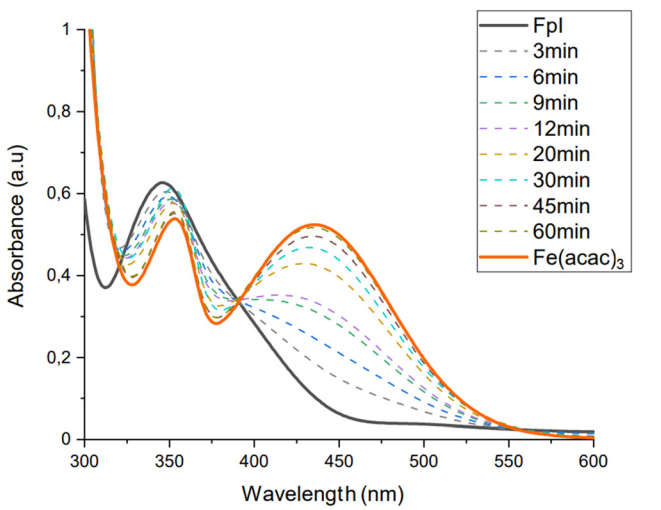

Fig. 1 Changes in UV–vis spectra during visible irradiation of an aerated solution of **1a** (0.3 mM), **2a** (0.9 mM), and DIPA (1.8 mM) in toluene at 0 °C; stars denote isosbestic points.

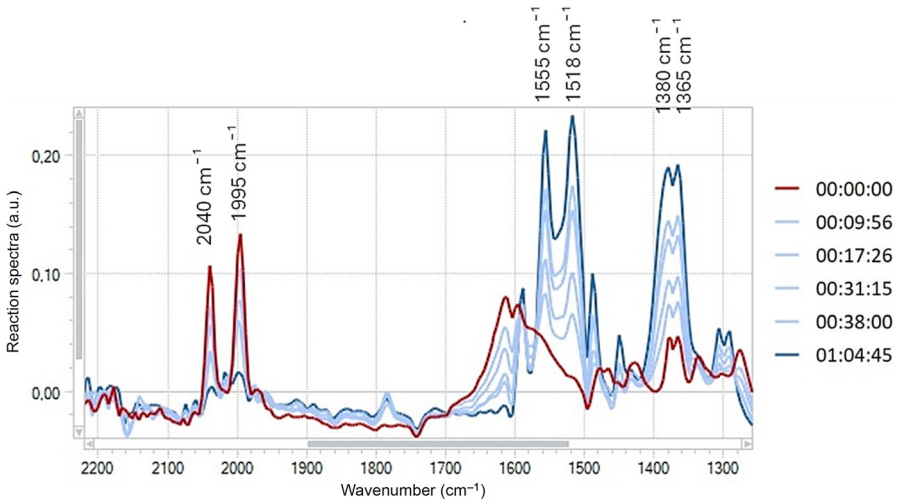

Fig. 2 Temporal evolution of the IR spectra of **1a** during its conversion to **3a** upon photolysis, as measured by the intensities of the bands at 2040 and 1995 cm^{-1} (**1a**) and those at 1555 and 1518 cm^{-1} (**3a**) (reaction time [hh : mm : ss]).

presence of isosbestic points[23] at 389 and 555 nm indicates that during the whole process, the photolyzed solution contained only these two iron-containing components. The spectra also intersect at about 340 nm, but without an isosbestic point. The lack of such a point is most likely related to the influence of absorption in this range by Hacac and $acac^-$ (λ_{max} = 270–290 nm), whose concentrations changed during photolysis.

The *in situ* IR study led to the same conclusion. The photolysis caused the disappearance of the absorption bands for the CO ligand of **1a** (2040 and 1995 cm^{-1}) and the appearance of intense absorption bands for **3a** (1555 and 1518 cm^{-1}; Fig. 2). The disappearance of the CO ligand bands was not accompanied by the appearance of any new absorption band in this spectral range. Fig. 3 shows the decay of **1a** (as represented by the bands at 2040 and 1995 cm^{-1}) and the formation of **3a** (*via* bands at 1555 and 1518 cm^{-1}). The sum of the intensities of both sets of bands shows little change with time, indicating that the reaction proceeded with no detectable intermediate. We believe that the reaction involved the rapid stepwise substitution of the ligands in **1a** with acac ligands (Scheme 3).

The first step of the reaction is the photochemical replacement of the iodido ligand with an acac anion to form complex **I**. The feasibility of the substitution is strongly supported by previous reports on similar photochemical substitutions of the iodido ligand in **1a** with anionic nitrogen ligands.[12,13,16,17,24,25] The suggested next step is intramolecular CO substitution, resulting in the formation of complex **II** with acac chelation (Scheme 3). The chelating acac ligand has been previously reported to behave as a non-innocent redox ligand.[26,27] This means that it can accept additional electron density from the

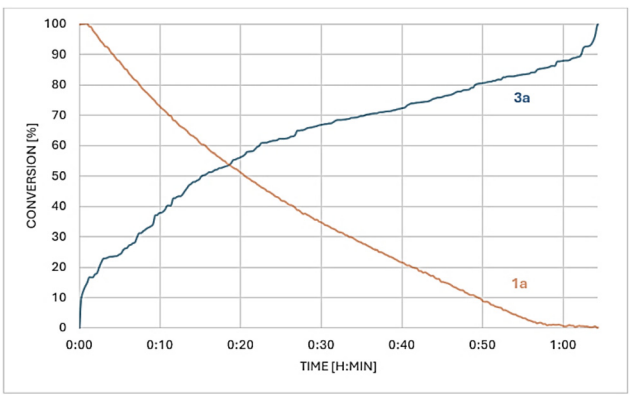

Fig. 3 Temporal evolution of the conversion of **1a** to **3a** during photolysis, as measured by the intensities of the bands at 2040 and 1995 cm^{-1} (**1a**) and those at 1555 and 1518 cm^{-1} (**3a**).

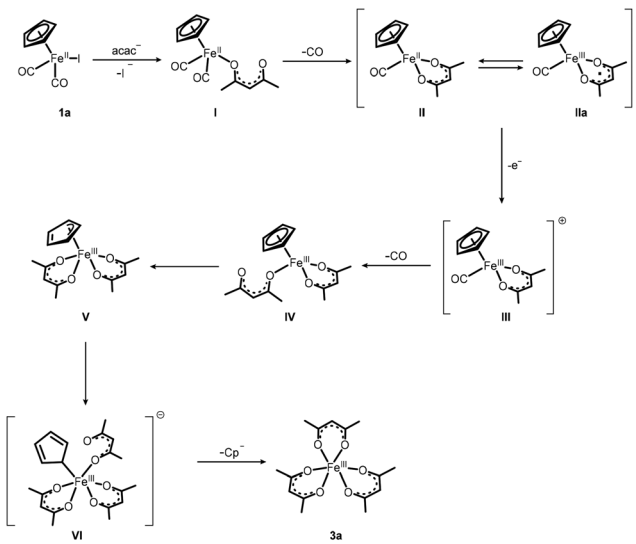

Scheme 3 Proposed reaction mechanism for the photoinduced transformation of **1a** to **3a**.

metal to increase its formal oxidation state.[28–33] Therefore, it can be assumed that complex **II** is in equilibrium with its valence tautomer **IIa**, which contains an Fe^{III} center and reactive $acac^{2-}$ anion radical.[34] This increase in electron density on the acac ligand might strengthen its reducing power to allow its oxidation by dioxygen or Hacac.

In the next step of the reaction the remaining CO ligand is replaced by the η^1-acac ligand, leading to complex **IV** and starting the sequence **IV** → **V** → **VI** → **3a**. This substitution is accompanied by the η^5-η^3-η^1 slippage of the Cp ligand.[35]

Reaction of 1a with other β-diketones

We also studied the reactions of the **1a**–DIPA system with other β-diketones (**2b–n**). Scheme 4 shows the results. The reaction proceeded with moderate-to-good yields for both aliphatic and aromatic diketones. β-Diketones possessing trifluoromethyl groups reacted more slowly with **1a** than the others. Most of the synthesized complexes have previously been obtained by established methods from metal halides; however, **3l** and **3m** have not been reported previously.

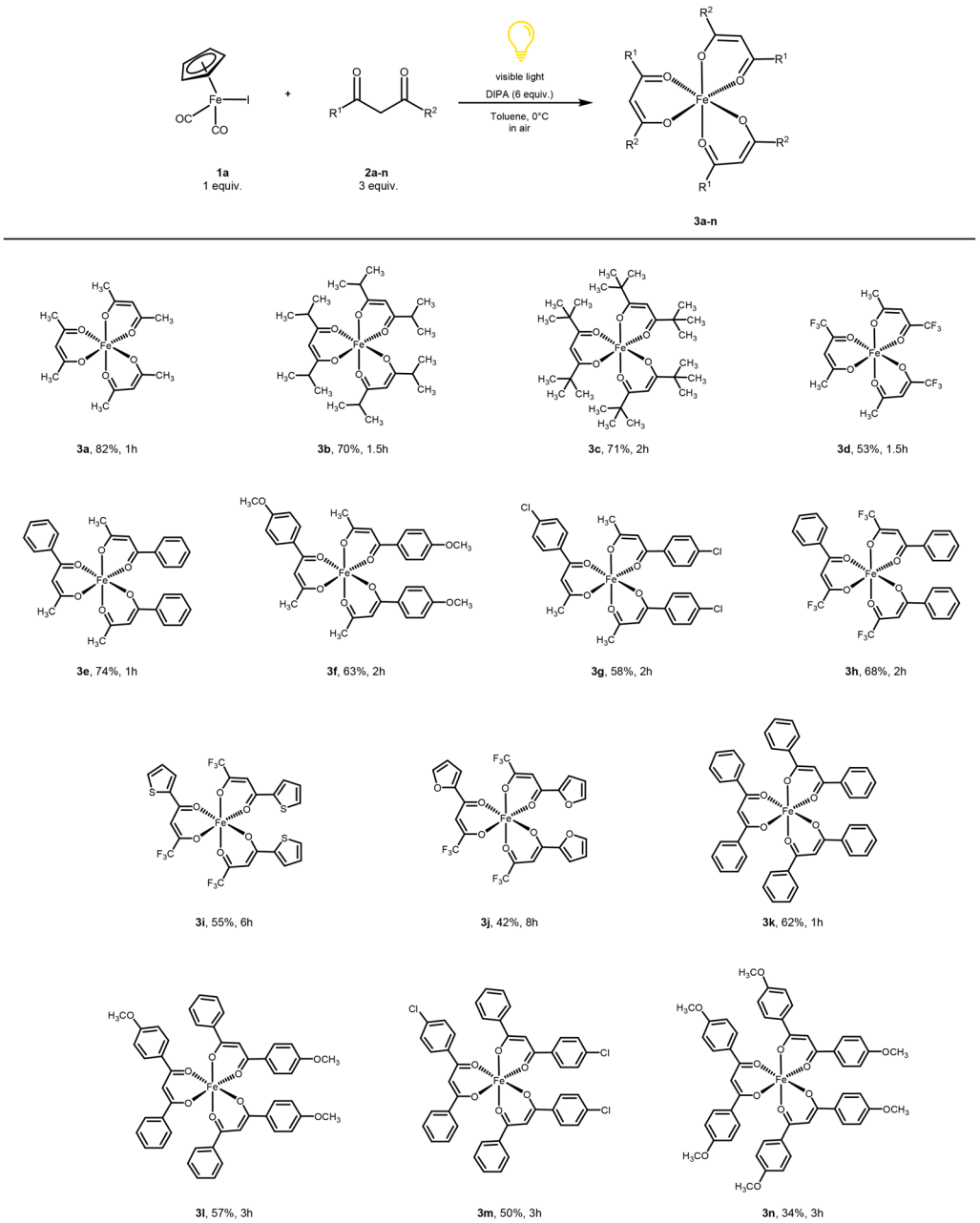

Scheme 4 Scope of the visible-light-induced reaction of **1a** with β-diketones **2a–n** and the yields of products. General conditions: **1a** (1 mmol), β-diketones **2a–n** (3 mmol), DIPA (6 mmol), toluene (10 mL), and four 100 W tungsten lamps.

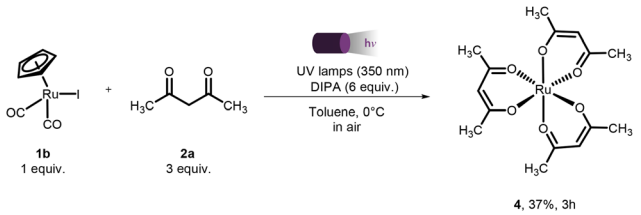

Scheme 5 Photochemical reaction of **1b** with **2a**.

We also tested the reaction using the ruthenium analogue of **1a**, $CpRu(CO)_2I$ (**1b**), and **2a**. In this case, however, the aerobic reaction under irradiation with visible light was slow and only 16% of the ruthenium(III) acetylacetonate **4** was isolated after 6 h. A higher yield was obtained in the reaction using UV light (350 nm). After 3h of irradiation, complex **4** was isolated in 37% yield (Scheme 5). Comparison of UV–vis absorption spectra of **1a** and **1b** provides a plausible explanation for the different photochemical reactivity of these compounds (Fig. 4). The spectrum of **1a** shows weak broad long-lying absorption bands with maxima at 500 and 648 nm, which were assigned to the symmetry-forbidden d–d transition.[16,17] Irradiation into these bands induces substitution of the iodido ligand in **1a** with the pyrrolyl anion. In contrast, the spectrum of **1b** shows negligible absorption in the range of 500–700 nm. Its lowest-energy band is observed at 423 nm, tailing into the UV region. Therefore, in this case UV irradiation is more strongly absorbed and more efficient.

Optimization of the reaction conditions is shown in Table 2.

Molecular structure of 3f

The tris(4-methoxybenzoylacetonato) iron complex **3f** crystallizes in a monoclinic system in the $P2_1/c$ space group. The asymmetric unit contains a single molecule of the complex

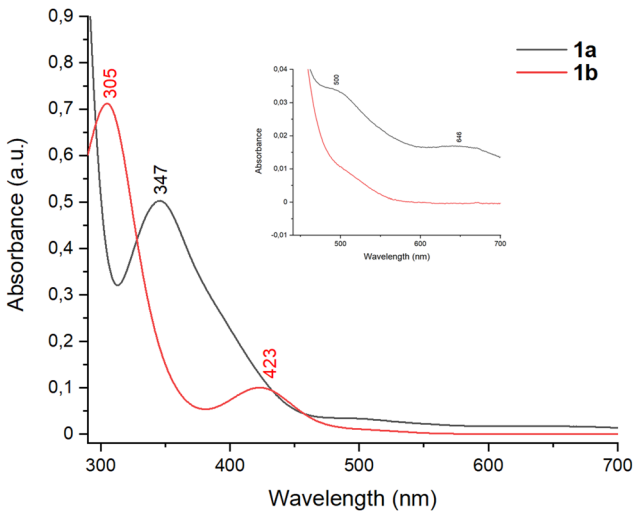

Fig. 4 UV–vis absorption spectra of **1a** and **1b** in toluene: c = 0.3 mM, 20 °C.

Table 2 Attempts to optimize the reaction conditions[a]

Entry	Deviation from general conditions	Yield **4**[b]
1	None	37%
2	No light	N.R.[c]
3	Visible light	16%[d]
4	Et_3N instead of DIPA	13%
5	DIPEA instead of DIPA	21%
6	THF instead of toluene	28%

[a] General conditions: **1b** (1 mmol), **2a** (3 mmol), DIPA (6 mmol), toluene (10 mL), 3 h, 0 °C. [b] Yield was based on isolated product. [c] N.R. = no reaction. [d] Time of reaction was 6 h.

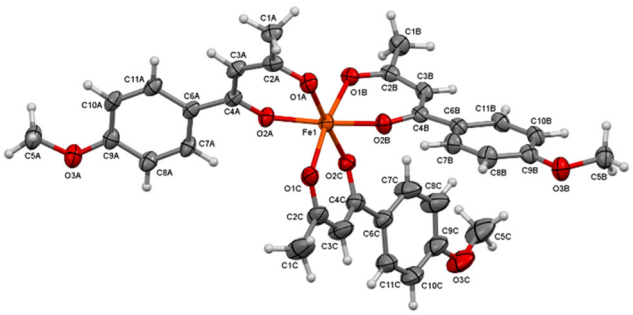

Fig. 5 Molecular structure of crystalline **3f**. Displacement ellipsoids are drawn at the 50% probability level.

presented in Fig. 5. The geometry of the complex molecule was calculated by Mercury 4.10,[36] and Table 3 lists selected geometrical parameters. The central iron ion coordinates with three 4-methoxybenzoylacetonato bidentate ligands. As the β-diketone ligand molecule is nonsymmetric, two stereoisomers are possible, one facial (*fac*) and the other meridional (*mer*). Analysis of the crystal structure revealed the latter stereoisomer, in agreement with previous reports suggesting that the *mer* isomer is energetically favorable.[37]

Additionally, a powder X-ray diffraction experiment conducted on a polycrystalline sample and a randomly selected bulk sample support that statement.

Fig. 6 presents a compilation of diffractograms for the single polycrystalline rosette, the crushed crystallites and the single crystal, calculated from the CIF file. The compilation is accompanied by photographs of the samples. A comparison of the measurements of the polycrystalline samples a and b reveals their phase to be identical. Moreover, a comparison with the calculated diffractogram demonstrates the corresponding order and size of the dominant reflections. The slight discrepancy in their positions can be attributed to the difference in measurement temperature; the monocrystal of the compound was measured at 100 K, while the polycrystals were measured at room temperature. The reduction in crystal lattice magnitude under low-temperature conditions resulted in an observed shift of the reflections by a few hundredths of angle 2Θ towards higher values, as would be expected.

Table 3 Crystal data and structure refinement

Identification code	**3f**
Empirical formula	$C_{33}H_{33}O_9Fe$
Formula weight	629.44
Crystal system	Monoclinic
Space group	$P2_1/c$
a	14.2832(7) Å
b	15.6780(8) Å
c	13.2979(5) Å
β	97.346(4)°
Volume	2953.4(2) Å^3
Z	4
ρ_{calc}	1.416 g cm^{-3}
μ	0.566 mm^{-1}
$F(000)$	1316
2Θ range for data collection	5.18° to 58.256°
Index ranges	$-19 \le h \le 19$, $-21 \le k \le 21$, $-16 \le l \le 18$
Reflections collected/ independent	33 711/7948 [R_{int} = 0.0405, R_{sigma} = 0.0346]
Data/restraints/parameters	7948/0/394
Goodness-of-fit on F^2	1.086
Final R indexes [$I > 2\sigma(I)$]	R_1 = 0.0668, wR_2 = 0.1732
Final R indexes [all data]	R_1 = 0.0850, wR_2 = 0.1857
Largest diff. peak/hole	0.62/−0.45 e Å^{-3}
CCDC no.	2371792†

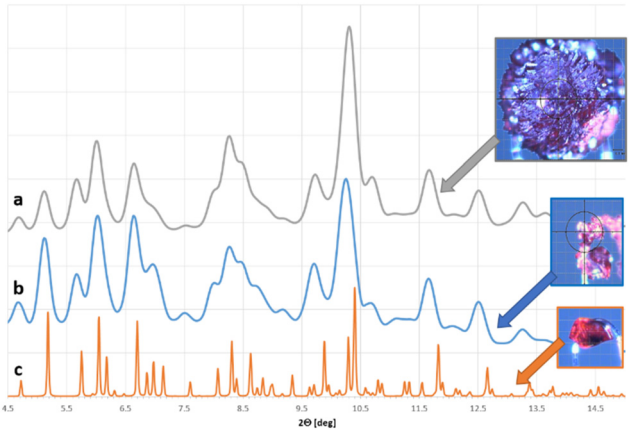

Fig. 6 The diffractograms of **3f**: a – single polycrystalline rosette; b – ground crystallites; c – calculated from the cif file of monocrystal measurements.

The overall coordination sphere can be described as a slightly distorted octahedron. The lengths of the Fe–O bonds are relatively constant (approximately 2.0 Å), with differences of less than 0.01 Å. Nevertheless, the coordination sphere is slightly distorted with regard to the O–Fe–O valence angles. Ligand C shows the greatest deviation from a right angle of approximately 5°, while ligands A and B exhibit an O–Fe–O valence angle of about 87°. As a result, the nominally linear arrangements of O1A–Fe1–O2C, O2A–Fe1–O2B, and O1B–Fe1–O1C showed slight deviations, with valence angles of approximately 177°, 171°, and 169°, respectively.

Conclusion

Complexes of the form $CpM(CO)_2I$ and their related dimers $[CpM(CO)_2]_2$ (M = Fe, Ru) are among the most commonly used starting materials in the synthesis of organometallic iron and ruthenium compounds. Their previously described photochemical transformations were limited to the substitution of the CO or I ligands. Here, we developed a new type of photochemical reaction in which all ligands were substituted with β-diketonate ligands and the central metal atom was oxidized. The reactions occurred under both anaerobic and aerobic conditions. A proposed reaction mechanism attributes the key role to the previously postulated non-innocent redox behavior of the acac$^-$ ligand. In contrast to previous studies focusing on the use of non-innocent ligands in catalysis, this paper suggests their potential utility in organometallic photochemistry.

Experimental section

Materials and methods

All chemicals and solvents were from commercial suppliers and used as received. Diketones **3a–3e** and **3h–3k** were purchased from Sigma-Aldrich, TCI and Ambeed and were used without any further purification. Reactions were carried out in air unless stated otherwise. TLC was performed on aluminum sheets precoated with silica gel (TLC silica gel 60 F_{254}, Merck). ^{1}H NMR spectra were recorded on a Bruker AVIII spectrometer (600 MHz) and are available in the ESI.† Chemical shifts are given relative to the residual non-deuterated peak for the $CDCl_3$ solvent (δ = 7.26 ppm for ^{1}H). IR spectra were recorded in KBr on a Fourier transform (FT)-IR spectrometer (NEXUS, Thermo Nicolet) and Shimadzu IR Spirit-T spectrometer. MS was performed with a Varian 500-MS LC IonTrap. Elemental analyses were conducted with a Vario EL III instrument (Elementar Analysensysteme GmbH). Melting points were determined in capillaries using a Stuart SMP30 apparatus, and are not corrected. Photochemical syntheses were carried out using four 100 W tungsten lamps and a UV lamp (TQ 150 Z3). *In situ* FT-IR measurements were performed on a Mettler-Toledo ReactIR 15 spectrometer equipped with a 9.5 mm AgX DiComp (diamond) probe and a liquid nitrogen-cooled MCT detector. The GC system (7820A, Agilent) was equipped with an automated sample injector (7693A, Agilent) and MS detector (5977B, Agilent Technologies, Waldbronn, Germany).

$CpFe(CO)_2I$ (**1a**) and $CpRu(CO)_2I$ (**1b**) were synthesized according to a previously published procedure.[38]

General procedure: photolysis of 1a with β-diketones and DIPA

A stirred solution of **1a** (304 mg, 1 mmol), β-diketone (3 mmol), and DIPA (840 µL, 6 mmol) in dry toluene (10 mL) was irradiated with visible light. The irradiated solution was externally cooled to 0 °C in a water-ice bath.

The initial black color of the solution became red upon irradiation. After the reaction was completed (1–8 h), silica gel

was added to the mixture. The solvent was evaporated *in vacuo*, and the crude reaction mixture was purified by flash column chromatography (CC; dry packing, hexane/dichloromethane/methanol eluent) to afford the corresponding product.

Tris(acetylacetonato)iron(III) 3a. Reaction time: 1 h. Dark red powder (291 mg, 82% yield). M.p.: 179–181 °C (lit. m.p. 180–182 °C).[39] CC (SiO_2, DCM/MeOH 95 : 5). For the **^{1}H NMR** spectrum see ESI Fig. S5.† **IR** (KBr, cm^{-1}) 2961, 2920, 1565, 1517, 1420, 1350, 1271, 1189, 1011, 927, 770, 665, 549. **ESI-MS** (*m*/*z*): 254.20 ([M-ligand]$^+$). Anal. calcd for $C_{15}H_{21}FeO_6$ (353.17): C 51.01, H 5.99; found: C 51.11, H 5.95.

Tris(2,6-dimethyl-3,5-heptanedionato)iron(III) 3b. Reaction time: 1.5 h. Dark orange solid (368 mg, 70% yield). M.p.: 97–100 °C (lit. m.p. 99 °C).[40] CC (SiO_2, hexane/DCM 1 : 9). For the **^{1}H NMR** spectrum see ESI Fig. S6.† **IR** (KBr, cm^{-1}) 2965, 2930, 2871, 1562, 1532, 1500, 1404, 1298, 1159, 1093, 922, 789, 690, 585. **ESI-MS** (*m*/*z*): 366.40 ([M-ligand]$^+$), 544.5 ([M + Na]$^+$). Anal. calcd for $C_{27}H_{45}FeO_6$: C 62.19, H 8.70; found: C 62.09, H 8.66.

Tris(2,2,6,6-tetramethyl-3,5-heptanedionato)iron(III) 3c. Reaction time: 2 h. Orange solid (431 mg, 71% yield). M.p.: 161–163 °C (lit. m.p. 163–164 °C).[41] CC (SiO_2, DCM/MeOH 99 : 1). For the **^{1}H NMR** spectrum see ESI Fig. S7.† **IR** (KBr, cm^{-1}) 2964, 2905, 2866, 1546, 1506, 1454, 1394, 1352, 1246, 1226, 1177, 1144, 872, 797, 623, 503. **ESI-MS** (*m*/*z*): 606.5 ([M + H]$^+$), 628.60 ([M + Na]$^+$). Anal. calcd for $C_{33}H_{57}FeO_6$: C 65.44, H 9.49; found: C 65.47, H 9.54.

Tris(trifluoroacetylacetonato)iron(III) 3d. Reaction time: 1.5 h. Red solid (274 mg, 53% yield). M.p.: 112–114 °C (lit. m.p. 113–116 °C).[39] CC (SiO_2, hexane/DCM 1 : 1). For the **^{1}H NMR** spectrum see ESI Fig. S8.† **IR** (KBr, cm^{-1}) 2934, 1606, 1523, 1506, 1452, 1365, 1283, 1225, 1192, 1130, 948, 861, 788, 729, 581, 502. **ESI-MS** (*m*/*z*): 538.20 ([M + Na]$^+$). Anal. calcd for $C_{15}H_{12}F_9FeO_6$: C 34.98, H 2.35; found: C 34.93, H 2.37.

Tris(benzoylacetonato)iron(III) 3e. Reaction time: 1 h. Red solid (401 mg, 74% yield). M.p.: 218–220 °C (lit. m.p. 220–221 °C).[42] CC (SiO_2, hexane/DCM 1 : 9). For the **^{1}H NMR** spectrum see ESI Fig. S9.† **IR** (KBr, cm^{-1}) 3058, 2993, 2964, 1588, 1544, 1508, 1487, 1449, 1378, 1357, 1306, 1292, 1207, 1180, 999, 959, 773, 715, 684, 576, 447. **ESI-MS** (*m*/*z*): 378.40 ([M-ligand]$^+$). Anal. calcd for $C_{30}H_{27}FeO_6$: C 66.80, H 5.05; found: C 66.83, H 4.98.

Tris(4-methoxybenzoylacetonato)iron(III) 3f. Reaction time: 2 h. Red solid (397 mg, 63% yield). M.p.: 108–111 °C (lit. m.p. 111–112 °C).[43] CC (SiO_2, hexane/DCM 1 : 9). For the **^{1}H NMR** spectrum see ESI Fig. S10.† **IR** (neat, cm^{-1}) 2924, 2840, 1583, 1521, 1492, 1417, 1352, 1291, 1250, 1169, 1113, 1024, 959, 842, 776, 637, 506. **ESI-MS** (*m*/*z*): 438.08 ([M-ligand]$^+$). Anal. calcd for $C_{33}H_{33}FeO_9$: C 62.97, H 5.28; found: C 62.90, H 5.29.

Tris(4-chlorobenzoylacetonato)iron(III) 3g. Reaction time: 2 h. Red solid (373 mg, 58% yield). M.p.: 185–188 °C (lit. m.p. 187–188 °C).[43] CC (SiO_2, hexane/DCM 1 : 9). For the **^{1}H NMR** spectrum see ESI Fig. S11.† **IR** (neat, cm^{-1}) 3006, 2971, 1580, 1509, 1483, 1404, 1354, 1294, 1173, 1091, 1011, 998, 956, 850, 779, 752, 594. **ESI-MS** (*m*/*z*): 446.20 ([M-ligand]$^+$). Anal. calcd for $C_{30}H_{24}Cl_3FeO_6$: C 56.06, H 3.76; found: C 56.19, H 3.79.

Tris(4,4,4-trifluoro-1-phenyl-1,3-butanedionato)iron(III) 3h. Reaction time: 2 h. Red solid (476 mg, 68% yield). M.p.: 62–64 °C (lit. m.p. 58–60 °C).[39] CC (SiO_2, DCM/MeOH 99 : 1). For the **^{1}H NMR** spectrum see ESI Fig. S12.† **IR** (KBr, cm^{-1}) 3140, 3066, 1596, 1570, 1453, 1323, 1294, 1251, 1197, 1142, 1073, 942, 776, 699, 638, 592, 538. **HRMS (ESI)** *m*/*z* calcd for $C_{30}H_{19}F_9FeO_6^+$ ([M + H]$^+$): 702.0387; found: 702.0387. Anal. calcd for $C_{30}H_{18}F_9FeO_6$: C 51.38, H 2.59; found: C 51.42, H 2.62.

Tris(2-thenoyltrifluoroacetonato)iron(III) 3i. Reaction time: 6 h. Red solid (398 mg, 55% yield). M.p.: 160–162 °C (lit. m.p. 158–161 °C).[39] CC (SiO_2, hexane/DCM 5 : 95). For the **^{1}H NMR** spectrum see ESI Fig. S13.† **IR** (KBr, cm^{-1}) 3113, 1567, 1540, 1508, 1404, 1350, 1308, 1255, 1232, 1192, 1136, 1066, 1014, 933, 862, 798, 730, 647, 588. **ESI-MS** (*m*/*z*): 498.20 ([M-ligand]$^+$), 742.30 ([M + Na]$^+$). Anal. calcd for $C_{24}H_{12}F_9FeO_6S_3$: C 40.07, H 1.68; found: C 40.10, H 1.56.

Tris(4,4,4-trifluoro-1-(2-furoyl)-1,3-butanedionato)iron(III) 3j. Reaction time: 8 h. Red solid (285 mg, 42% yield). M.p.: 202–205 °C (lit. m.p. 205–208 °C).[39] CC (SiO_2, hexane/DCM 1 : 9). For the **^{1}H NMR** spectrum see ESI Fig. S14.† **IR** (KBr, cm^{-1}) 3153, 3125, 1593, 1574, 1458, 1437, 1311, 1261, 1199, 1150, 1138, 1097, 1018, 945, 883, 862, 772, 679, 591. **ESI-MS** (*m*/*z*): 466.20 ([M-ligand]$^+$), 694.20 ([M + Na]$^+$). Anal. calcd for $C_{24}H_{12}F_9FeO_9$: C 42.95, H 1.80; found: C 43.01, H 1.65.

Tris(dibenzoylmethanato)iron(III) 3k. Reaction time: 1 h. Red solid (452 mg, 62% yield). M.p.: 251–253 °C (lit. m.p. 253–255 °C).[42] CC (SiO_2, hexane/DCM 1 : 9). For the **^{1}H NMR** spectrum see ESI Fig. S15.† **IR** (KBr, cm^{-1}) 3055, 3025, 2964, 1590, 1529, 1522, 1478, 1452, 1380, 1359, 1315, 1225, 1180, 1066, 1024, 939, 757, 721, 686, 621, 548. **HRMS (ESI)** *m*/*z* calcd for $C_{45}H_{34}FeO_6^+$ ([M + H]$^+$): 726.1705; found: 726.1722. Anal. calcd for $C_{45}H_{33}FeO_6$: C 74.49, H 4.58; found: C 74.60, H 4.51.

Tris(benzoyl-4-methoxybenzoylmethanato)iron(III) 3l. Reaction time: 3 h. Red solid (467 mg, 57% yield). M.p.: 86–88 °C. CC (SiO_2, hexane/DCM 1 : 9). For the **^{1}H NMR** spectrum see ESI Fig. S16.† **IR** (neat, cm^{-1}) 2955, 2924, 2853, 1601, 1586, 1519, 1498, 1476, 1447, 1374, 1355, 1298, 1253, 1222, 1169, 1022, 936, 842, 789, 711, 691, 603, 531. **HRMS (ESI)** *m*/*z* calcd for $C_{48}H_{40}FeO_6^+$ ([M + H]$^+$): 816.2022; found: 816.2003. Anal. calcd for $C_{48}H_{39}FeO_9$: C 70.68, H 4.82; found: C 70.64, H 4.86.

Tris(1-(4-chlorophenyl)-3-phenyl-1,3-propanedionato)iron(III) 3m. Reaction time: 3 h. Dark red solid (418 mg, 50% yield). M.p.: 262–265 °C. CC (SiO_2, hexane/DCM 1 : 9). For the **^{1}H NMR** spectrum see ESI Fig. S17.† **IR** (neat, cm^{-1}) 3056, 3030, 1737, 1587, 1511, 1475, 1446, 1403, 1351, 1311, 1295, 1221, 1090, 1011, 937, 793, 763, 685, 636, 535. **ESI-MS** (*m*/*z*): 570.30 ([M-ligand]$^+$). Anal. calcd for $C_{45}H_{30}Cl_3FeO_6$: C 65.20, H 3.65; found: C 65.13, H 3.52.

Tris[di(4-methoxy)benzenecarbonylmethanato]iron(III) 3n. Reaction time: 3 h. Dark red solid (306 mg, 34% yield). M.p.: 283–286 °C (lit. m.p. 285–289 °C).[42] The product was obtained by trituration from dichloromethane and diethyl ether (pre-cooled to −20 °C) as a dark red solid. For the **^{1}H NMR** spec-

trum see ESI Fig. S18.† **IR** (neat, cm^{-1}) 3006, 2970, 2937, 2836, 1600, 1584, 1525, 1489, 1459, 1379, 1364, 1296, 1253, 1224, 1180, 1125, 1103, 1016, 847, 787, 645, 515, 471. **HRMS (ESI)** *m*/*z* calcd for $C_{51}H_{46}FeO_{12}^{+}$ ($[M + H]^+$): 906.2339; found: 906.2348. Anal. calcd for $C_{51}H_{45}FeO_{12}$: C 67.63, H 5.01; found: C 67.40, H 5.11.

Synthesis of ruthenium complex 4

A stirred solution of **1b** (350 mg, 1 mmol), Hacac (1050 mg, 3 mmol) and DIPA (840 μl, 6 mmol) in dry toluene (10 mL) was irradiated with 350 nm UV light. The irradiated solution was externally cooled to 0 °C in a water-ice bath. The initial orange color of the solution turned red upon irradiation. The reaction reached completion after 4 h, and silica gel was added to the mixture. The solvent was evaporated *in vacuo*, and the crude reaction mixture was purified by flash column chromatography (dry packing, hexane/dichloromethane/methanol as eluent) to afford the corresponding product.

Tris(acetylacetonato)ruthenium(III) 4. Dark orange solid (150 mg, 37% yield). M.p.: 228–231 °C (lit. m.p. 223 °C).[2] CC (SiO_2, DCM/MeOH 95 : 5). For the **^{1}H NMR** spectrum see ESI Fig. S19.† **IR** (KBr, cm^{-1}) 2997, 2919, 1541, 1516, 1375, 1364, 1268, 1018, 934, 778, 622, 454 cm^{-1}. **ESI-MS** (*m*/*z*): 400.30 ($[M + H]^+$). Anal. calcd for $C_{15}H_{21}RuO_6$: C 45.22, H 5.31; found: C 45.05, H 5.24.

In situ FT-IR analysis

The reaction between **1a** and acetylacetone **2a** was monitored by *in situ* FT-IR spectroscopy. Acetylacetone (3 mmol), **1a** (1 mmol), and dry toluene (10 mL) were stirred for 5 min in a 25 mL tube equipped with a magnetic stirring bar and 9.5 mm AgX DiComp (diamond) probe. DIPA (6 mmol) was added, and the reaction mixture was stirred under irradiation (four 100 W tungsten lamps) at 0 °C. Spectra were acquired with a resolution of 4 cm^{-1} collecting scans for each spectrum at 15 s intervals for 1 h.

X-ray structure determination

Crystals of **3f** were obtained from dichloromethane/heptane at room temperature. Crystals exhibited a propensity to grow in rosette/lenticular-like structures (Fig. S4†). In order to ascertain the phase purity of the crystals X-ray powder experiments were conducted. Two measurements were recorded: the first for a polycrystalline rosette, and the second for a group of crystals extracted from a different area of the vial. These crystals were then subjected to a crushing process in an agate mortar prior to their application to the nylon loop. X-ray data were collected on an Oxford Diffraction SuperNova DualSource diffractometer with the use of a monochromated Mo Kα X-ray source (λ = 0.71073 Å) at room temperature. For the single-crystal experiment, the selected crystal was mounted on a loop for X-ray measurement and kept at 100 K during data collection. Data reduction and analytical absorption correction were performed with CrysAlis PRO.[44] Using Olex2,[45] the structure was solved with the SHELXT[46] structure solution program using intrinsic phasing and refined with the SHELXL[47] refinement package using least squares minimization.

The non-hydrogen atoms were refined anisotropically. Hydrogen atoms were introduced in calculated positions with idealized geometry and constrained using a rigid-body model with isotropic displacement parameters equal to 1.2 and 1.5 in the case of CH and CH_3 hydrogen atoms, respectively. Table 3 summarizes the relevant crystallographic data.

Author contributions

S.J.: (organic synthesis) methodology, investigation, manuscript writing; C.D.: (organic synthesis) investigation; D.J.: (organic synthesis) investigation; J.W.: (IR measurements); K. S-K.: (IR measurements); S.W.: (crystallography) investigation; J.Z.: conceptualization, manuscript writing; B.R.: conceptualization, supervision, manuscript writing.

Data availability

The data supporting this article have been included as part of the ESI.† Crystallographic data for **3f** has been deposited at the CCDC under 2371792.†

Conflicts of interest

There are no conflicts to declare.

Acknowledgements

This work was financially supported by the Faculty of Chemistry of the University of Lodz, Poland. Funding for this research was provided by the EFRD's Operational Programme – Development of Eastern Poland 2007–2013 (Project No. POPW.01.03.00-20-004/11, for the Oxford Diffraction SuperNova Dual Source diffractometer). The authors thank Prof. Łukasz Półtorak for the opportunity to perform IR spectra using the Shimadzu IR Spirit-T spectrometer.

References

1 N. J. Coville, E. A. Darling, A. W. Hearn and P. Johnston, *J. Organomet. Chem.*, 1987, **328**, 375–385.
2 P.-M. Treichel, R. Shubkin, K. Barnett and D. Reichard, *Inorg. Chem.*, 1966, **5**, 1177–1181.
3 V. V. Verpekin, O. V. Semeikin, A. D. Vasiliev, A. A. Kondrasenko, Y. A. Belousov and N. A. Ustynyuk, *RSC Adv.*, 2020, **10**, 17014–17025.
4 Y.-C. Lin, Z.-Y. Ke, P.-H. Liao, C.-Y. Tseng and K. V. Kong, *Chem. Commun.*, 2020, **56**, 936–939.
5 T. Pradeep, M. Velusamy and R. Mayilmurugan, *Mol. Catal.*, 2018, **459**, 71–77.

6 A. Pilon, A. R. Brás, L. Côrte-Real, F. Avecilla, P. J. Costa, A. Preto, M. H. Garcia and A. Valente, *Molecules*, 2020, **25**, 1592.
7 A. Pilon, P. Gírio, G. Nogueira, F. Avecilla, H. Adams, J. Lorenzo, M. H. Garcia and A. Valente, *J. Organomet. Chem.*, 2017, **852**, 34–42.
8 D. H. Gibson, W.-L. Hsu and F. U. Ahmed, *J. Organomet. Chem.*, 1981, **215**, 379–401.
9 G. Bresciani, S. Volante, L. Biancalana, S. Zacchini, G. Pampaloni and F. Marchetti, *J. Organomet. Chem.*, 2023, **1001**, 122851.
10 N. J. Coville, E. A. Darling, A. W. Hearn and P. Johnston, *J. Organomet. Chem.*, 1987, **328**, 375–385.
11 D. G. Alway and K. W. Barnett, *Inorg. Chem.*, 1978, **17**, 2826–2831.
12 J. Zakrzewski, *J. Organomet. Chem.*, 1987, **327**, C41–C42.
13 J. Zakrzewski, *J. Organomet. Chem.*, 1989, **359**, 215–218.
14 A. Vessières, K. Kowalski, J. Zakrzewski, A. Stepien, M. Grabowski and G. Jaouen, *Bioconjugate Chem.*, 1999, **10**, 379–385.
15 J. Zakrzewski and M. Pawlak, *J. Organomet. Chem.*, 1998, **568**, 171–175.
16 C. E. Borja, V. Jakúbek and A. J. Lees, *Inorg. Chem.*, 1998, **37**, 2281–2284.
17 A. J. Lees, *Coord. Chem. Rev.*, 2001, **211**, 255–278.
18 J. Zakrzewski, *J. Organomet. Chem.*, 1991, **412**, C23–C26.
19 S. Kawaguchi, *Coord. Chem. Rev.*, 1986, **70**, 51–84.
20 C. Pettinari, F. Marchetti and A. Drozdov, in *Comprehensive Coordination Chemistry II*, ed. J. A. McCleverty and T. J. Meyer, Pergamon, Oxford, 2003, pp. 97–115.
21 D. T. Sawyer and J. S. Valentine, *Acc. Chem. Res.*, 1981, **14**, 393–400.
22 T. E. Neal and R. W. Murray, *Anal. Chem.*, 1970, **42**, 1654–1656.
23 F. Kaspar, *ChemBioChem*, 2023, **24**, e202200744.
24 B. Rudolf and J. Zakrzewski, *Tetrahedron Lett.*, 1994, **35**, 9611–9612.
25 B. Rudolf, M. Salmain, E. Fornal and A. Rybarczyk-Pirek, *Appl. Organomet. Chem.*, 2012, **26**, 80–85.
26 M. G. Vinum, L. Voigt, C. Bell, D. Mihrin, R. W. Larsen, K. M. Clark and K. S. Pedersen, *Chem. – Eur. J.*, 2020, **26**, 2143–2147.
27 M. G. Vinum, L. Voigt, S. Hansen, C. Bell, K. M. Clark, R. W. Larsen and K. Pedersen, *Chem. Sci.*, 2020, **11**, 8267–8272.
28 M. Zou and K. M. Waldie, *Inorg. Chem. Front.*, 2024, **11**, 5795–5809.
29 V. Lyaskovskyy and B. de Bruin, *ACS Catal.*, 2012, **2**, 270–279.
30 M. Sutradhar, A. J. Pombeiro and J. A. L. da Silva, *Coord. Chem. Rev.*, 2021, **439**, 213911.
31 B. de Bruin, P. Gualco and N. D. Paul, *Ligand Design in Metal Chemistry: Reactivity and Catalysis*, 2016, pp. 176–204.
32 R. Mondal, A. K. Guin, G. Chakraborty and N. D. Paul, *Org. Biomol. Chem.*, 2022, **20**, 296–328.
33 B. Mondal and S. Ye, *Coord. Chem. Rev.*, 2020, **405**, 213115.
34 A. Staško, A. Tkáč, V. Laurinc and L. Malík, *Org. Magn. Reson.*, 1976, **8**, 237–239.
35 J. M. O'Connor and C. P. Casey, *Chem. Rev.*, 1987, **87**, 307–318.
36 P. R. Edgington, P. McCabe, C. F. Macrae, E. Pidcock, G. P. Shields, R. Taylor, M. Towler and J. Van De Streek, *J. Appl. Crystallogr.*, 2006, **39**, 453–457.
37 M. M. Conradie, P. H. van Rooyen and J. Conradie, *J. Mol. Struct.*, 2013, **1053**, 134–140.
38 B. F. Hallam and P. L. Pauson, *J. Chem. Soc.*, 1956, 3030–3037.
39 M. M. Conradie, *Molecules*, 2022, **27**, 3743.
40 J. C. Lo, J. Gui, Y. Yabe, C. M. Pan and P. S. Baran, *Nature*, 2014, **516**, 343–348.
41 K. M. Armstrong and P. Kilian, *Eur. J. Inorg. Chem.*, 2011, **2011**, 2138–2147.
42 F. Puls, P. Linke, O. Kataeva and H. J. Knölker, *Angew. Chem., Int. Ed.*, 2021, **60**, 14083–14090.
43 H. Imai and H. Tamura, *Nippon Kagaku Kaishi*, 1989, **6**, 967–971.
44 *Rigaku Oxford Diffraction, (2020), CrysAlisPro Software system, version 1.171.41.123a*, Rigaku Corporation, Wroclaw, Poland.
45 O. V. Dolomanov, L. J. Bourhis, R. J. Gildea, J. A. K. Howard and H. Puschmann, *J. Appl. Crystallogr.*, 2009, **42**, 339–341.
46 G. M. Sheldrick, *Acta Crystallogr., Sect. A:Found. Adv.*, 2015, **71**, 3–8.
47 G. M. Sheldrick, *Acta Crystallogr.*, 2008, **64**, 112–122.